CrystEngComm

Synthesis, Structural Characterization, and Luminescent Properties of Heteroleptic Bismuth-Organic Compounds

Journal:	*CrystEngComm*
Manuscript ID	CE-ART-09-2021-001242.R1
Article Type:	Paper
Date Submitted by the Author:	27-Oct-2021
Complete List of Authors:	Adcock, Alyssa; Georgetown University, Department of Chemistry Marwitz, Alexander; Georgetown University, Department of Chemistry Sanz, Lulio; Georgetown University, Department of Chemistry Ayscue, Russell; Georgetown University, Department of Chemistry Bertke, Jeffery; Georgetown University, Department of Chemistry Knope, Karah; Georgetown University, Department of Chemistry

Synthesis, Structural Characterization, and Luminescent Properties of Heteroleptic Bismuth-Organic Compounds

*Alyssa K. Adcock, Alexander C. Marwitz, Lulio A. Sanz, R. Lee Ayscue III, Jeffery A. Bertke, and Karah E. Knope**

Department of Chemistry, Georgetown University, 37th and O Streets, NW, Washington, D.C. 20057, USA

KEYWORDS: Bismuth; europium doping; terpyridine; β-diketonates; luminescence

ABSTRACT

Four heteroleptic bismuth-organic phases bearing 2,2';6',2''-terpyridine (terpy) and 2-thenoyltrifluoroacetone (TTA) of the general formula $[BiX_y(TTA)_{3-y}(terpy)]$, where X = NO_3 (**2**), Cl (**3**), Br (**4**), Br_2 (**5**), were synthesized at room temperature. A minor phase, $[Bi_2(terpy)_2(MeO)_2(NO_3)_4]$ (**1**), formed in the same reaction as **2**, and was manually separated to afford a phase pure sample of **2**. The structures were determined through single crystal X-ray diffraction, and further characterized via powder X-ray diffraction, Raman spectroscopy, and thermogravimetric analysis. The structures of **2** – **5** are built from discrete monomeric units, whereas **1** contains dimeric complexes. Significant π-π stacking and halide-π interactions are observed in the solid-state structures. Europium-doped phases of **2 - 5** were synthesized through addition of an aliquot of a europium nitrate or europium chloride solution to the initial reaction solution. For comparison, $[EuNO_3(TTA)_2(terpy)]\cdot 0.3MeOH$ (**6**), which is isostructural to **2**, was synthesized. Photophysical measurements were carried out for each of the lanthanide containing phases, and quantum yield and lifetime values were determined for the visible-light emitters. The synthesis, structural chemistry, and spectroscopic properties of the phases are presented.

INTRODUCTION

Luminescent materials are ubiquitous in modern society.[1-6] The development of novel platforms for luminescent compounds with attractive photophysical properties continues to draw significant interest;

there is wide recognition that these materials are critical to meeting our growing energy, lighting, and security needs. Within this context, our group and others have looked towards developing a better understanding of structure-property relationships in bismuth-based compounds and in some cases, their lanthanide-doped analogs. [7-11] Bismuth-based materials offer rich structural diversity and properties that can be tailored towards a wide array of applications from medicine to catalysis to optics.[12-20] Yet the synthesis, characterization, and application of bismuth-based materials remains underdeveloped as compared to those built from more heavily researched metals, such as transition metals. For example, a cursory search of the Cambridge Structural Database (Version 5.42, May 2021 update) yields ca. 4,650 hits for bismuth containing compounds.[21] For context, there are over 60,500 hits for iron, approximately 79,000 results for copper, and even approximately 5,550 hits for europium.[21] This lack of Bi-organic compounds is perhaps due, in part, to the limited solubility of bismuth salts and their hydrolytic instability, which complicate rationale design strategies. [22] Moreover, the flexible coordination environment of bismuth, arising from the $6s^2$ lone pair electrons further complicates structure prediction and rationale design. [23-27] Yet the global availability (i.e. low cost) and relatively low toxicity of bismuth, as compared to other heavy elements,[28] coupled with its unique lone pair electron effects, and potential for structural regulation of light emission and detection warrant the development of effective synthetic routes towards bismuth-based materials and the examination of the photophysical properties thereof.

Bi-organic compounds are attractive targets for photoluminescent materials design.[11, 19, 24, 25, 29-38] Homometallic bismuth-organic compounds have been shown to exhibit promising luminescence behavior, with emission extending across the visible region and even approaching white light emission. [7, 10, 39, 40 24] Lanthanide doping into Bi-organic hosts has been harnessed to achieve effective lanthanide sensitization and line-like emission characteristic of the lanthanide ions.[9, 23, 30, 32, 36, 41-44] The broadband emission of Bi-organic compounds together with the line-like emission of lanthanide ions has been capitalized on to achieve color tuning in lanthanide-doped Bi-organic materials.[11] However, there remains a lack of

understanding of the fundamental structure-property relationships that underpin the photophysical properties of homo- and heterometallic bismuth based materials. As demonstrated by previous work from our group, the lack of Bi- and Ln- structural analogs [9,45] can make comparison of the photophysical properties of Ln-doped and Ln-only phases difficult as analogous reactions often give rise to unique coordination environments about the bismuth and lanthanide metal ions; this precludes a proper assessment of the utility of bismuth based materials to serve as hosts for lanthanide metal ions, while retaining the notable emission of the lanthanides.

As such, we have turned towards a bismuth system incorporating both 2-thenoyltrifluoroacetone (TTA) and 2,2';6',2"-terpyridine (terpy) ligands. Terpy and other aromatic N-donor ligands have been heavily studied in Ln-based compounds[46] and we have seen successful sensitization through its use coupled with thiophenecarboxylate. Furthermore, β-diketonates are another class of effective Ln sensitizers,[47-49] and we hypothesized that the push-pull effect that TTA offers could help minimize the effect of the bismuth lone pair towards the isolation of isomorphous Bi- and Eu- phases. We herein report the synthesis and characterization of several bismuth- and europium-TTA-terpy compounds. Notably, using this approach we have isolated isostructural homometallic Bi- and Eu- complexes. Europium doping of the bismuth-only phases was examined and despite similarities in the coordination chemistry of the Bi and Eu metal centers, limited Eu incorporation into the parent Bi host phases was observed. The synthesis, characterization, and photophysical properties of the compounds are described.

EXPERIMENTAL SECTION

Materials

All starting materials were commercially available and used without any further purification. $Bi(NO_3)_3 \cdot 5H_2O$ (Fisher, 99.2%), $BiCl_3$ (Acros Organic, 98+%), $BiBr_3$ (Alfa Aesar, 99%), $Eu(NO_3)_3 \cdot 6H_2O$ (BeanTown Chemical, 99.9%), $EuCl_3$ (Aldrich Chemicals Co., 99.9%), 2-thenoyltrifluoroacetone (Fisher,

99%), 2,2';6',2''-terpyridine (Alfa Aesar, 97%), potassium hydroxide (Ward's Science), ethanol (Warner Graham Company), and methanol (Fisher) were used as received.

Stock solutions. A solution of 1 M potassium hydroxide was prepared in methanol. Solutions of 0.1 M europium nitrate or europium chloride in methanol were prepared and used in the synthesis of the doped phases.

$[Bi_2(terpy)_2(MeO)_2(NO_3)_4]$ (1) and $[BiNO_3(TTA)_2(terpy)]$ (2)

Bismuth nitrate (0.0242 grams, 0.05 mmol), TTA (0.0222 grams, 0.1 mmol), terpy (0.0112 grams, 0.05 mmol), and methanol (3 mL) were loaded into a 10 mL glass vial. The pH was adjusted to ca. 6-7 by addition of 1 M potassium hydroxide (100 µL). The glass vial was then capped and placed on the benchtop under ambient conditions. Crystallization was observed almost immediately. After two days, the products were filtered, washed in ethanol, and allowed to dry. Small colorless blocks of **1** (minor phase) along with beige plates of **2** were collected (Fig. S7). Manual separation allowed for further characterization of **2** (Fig. S7). Elemental Analysis for (**2**) $C_{31}H_{19}BiF_6N_4O_7S_2$: Calc. (Obs.): C, 39.33 (39.13); H, 2.02 (1.99); N, 5.92 (5.88 %). Raman for (**1**): ῡ = 310, 326, 427, 449, 657, 724, 1010, 1021, 1043, 1053, 1261, 1276, 1291, 1332, 1461, 1482, 1498, 1567, 1574, 1595 cm^{-1}; (**2**): ῡ = 250, 307, 319, 608, 645, 655, 684, 723, 753, 830, 931, 1015, 1034, 1060, 1083, 1300, 1332, 1358, 1414, 1485, 1500, 1520, 1596 cm^{-1}.

$[BiCl(TTA)_2(terpy)]$ (3)

Bismuth chloride (0.0158 grams, 0.05 mmol), TTA (0.0222 grams, 0.1 mmol), terpy (0.0112 grams, 0.05 mmol), and methanol (2.9 mL) were loaded into a 10 mL glass vial. The pH was increased to ~6 with 1 M potassium hydroxide in methanol (100µL). A yellowish-white microcrystalline solid precipitated immediately from solution upon addition of the reactants. The glass vial was then capped and placed on the benchtop under ambient conditions. After one week, the products were filtered, washed in ethanol, and allowed to dry. Yellow blocks and a microcrystalline powder of **3** were collected (Fig. S8). Yield: 49% (based on Bi). Elemental Analysis for (**3**) $C_{31}H_{19}BiClF_6N_3O_4S_2$: Calc. (Obs.): C, 40.46 (39.97); H, 2.08 (2.04); N, 4.57 (4.57 %). Raman ῡ = 210, 234, 312, 453, 654, 678, 724, 751, 930, 1016, 1043, 1058, 1072, 1089, 1245, 1290, 1333, 1357, 1409, 1435, 1513, 1573, 1601 cm^{-1}.

$[BiBr(TTA)_2(terpy)]$ (4)

Bismuth bromide (0.022 grams, 0.05 mmol), TTA (0.0222 grams, 0.1 mmol), terpy (0.0112 grams, 0.05 mmol), and methanol (3 mL) were loaded into a 10 mL glass vial. The pH was increased to ca. 5-6 with 1 M potassium hydroxide in methanol (100µL). A yellowish-white microcrystalline solid precipitated immediately from solution upon addition of the reactants. The glass vial was then capped and placed on the

benchtop under ambient conditions. After one week, the products were filtered, washed in ethanol, and allowed to dry. Yellow rods and a microcrystalline powder of **4** were collected (Fig. S9). Yield: 69% (based on Bi). Elemental Analysis for (**4**) $C_{31}H_{19}BiBrF_6N_3O_4S_2$: Calc. (Obs.): C, 38.60 (38.24); H, 1.99 (1.88); N, 4.36 (4.20 %). Raman $\tilde{\upsilon}$ = 211, 245, 312, 452, 643, 679, 723, 751, 766, 930, 1016, 1043, 1058, 1071, 1089, 1107, 1246, 1290, 1331, 1357, 1409, 1435, 1518, 1591 cm^{-1}.

[$BiBr_2$(TTA)(terpy)] (5)

Bismuth bromide (0.022 grams, 0.05 mmol), TTA (0.0111 grams, 0.05 mmol), terpy (0.0112 grams, 0.05 mmol), and methanol (2.9 mL) were loaded into a 10 mL glass vial. The pH was increased to ca. 5-6 with 1 M potassium hydroxide in methanol (100 μL). A yellowish-white microcrystalline solid precipitated immediately from solution upon addition of the reactants. The glass vial was capped and placed on the benchtop at room temperature. After one week, the products were filtered, washed in ethanol, and allowed to dry. Yellow rods and a microcrystalline powder of **5** were collected (Fig. S10). Yield: 66% (based on Bi). Elemental Analysis for (**5**) $C_{23}H_{15}BiBr_2F_3N_3O_2S$: Calc. (Obs.): C, 33.56 (33.55); H, 1.84 (1.92); N, 5.10 (5.05 %). Raman $\tilde{\upsilon}$ = 216, 248, 264, 311, 644, 654, 684, 723, 755, 799, 828, 929, 1013, 1042, 1061, 1075, 1105, 1298, 1328, 1338, 1406, 1428, 1458, 1482, 1497, 1567, 1592 cm^{-1}.

[$EuNO_3$$(TTA)_2$(terpy)]·0.3MeOH (6)

Europium nitrate (0.0223 grams, 0.05 mmol), TTA (0.0222 grams, 0.1 mmol), terpy (0.0112 grams, 0.05 mmol), and methanol (3 mL) were loaded into a 10 mL glass vial. The pH was increased to ca. 6-7 with 1 M potassium hydroxide in methanol (100 μL). The glass vial was then capped and placed on the benchtop under ambient conditions. Crystallization was observed after a few days. After two weeks, the products were filtered, washed in ethanol, and allowed to dry. Colorless thick needles of **6** were collected (Fig. S11). Yield: 43% (based on Eu). Elemental Analysis for (**6**) $C_{31.3}H_{20.2}EuF_6N_4O_{7.3}S_2$: Calc. (Obs.): C, 41.80 (41.10); H, 2.26 (1.99); N, 6.23 (5.88 %). Raman for (**6**): $\tilde{\upsilon}$ = 216, 249, 269, 300, 604, 627, 641, 653, 682, 724, 751, 830, 936, 1013, 1035, 1044, 1061, 1082, 1287, 1331, 1351, 1412, 1500, 1518, 1571, 1598, 1630 cm^{-1}.

Doping

The europium doped samples of **2 – 5** were prepared by adding an aliquot of europium nitrate (**2**, **4** – **5**) or chloride (**3**) solution *vide infra* to the reactions just prior to crystallization of the bismuth-only phases. For **2**, the europium solution was added during the initial reaction set-up. For **3** – **5**, europium was added an

hour after the reaction solutions were prepared. When the europium solution was added at the beginning of the reaction, no Eu incorporation was observed based on visual inspection under a UV lamp.

[$Bi_{0.97}Eu_{0.03}NO_3(TTA)_2$(terpy)] ($Bi_{0.97}Eu_{0.03}$-2)

Bismuth nitrate (0.0218 grams, 0.045 mmol), TTA (0.0222 grams, 0.1 mmol), terpy (0.0112 grams, 0.05 mmol), and methanol (3 mL) were loaded into a 10 mL glass vial. The pH was increased to ca. 6-7 with 1 M potassium hydroxide in methanol (100 μL). An aliquot of 0.1 M europium nitrate in methanol (50 μL, 0.005 mmol) was immediately added to the vial. The glass vial was then capped and placed on the benchtop under ambient conditions. Crystallization was immediately observed. After two days, the products were filtered, washed in ethanol, and allowed to dry. Beige plates of compound **$Bi_{0.97}Eu_{0.03}$-2** were collected with no apparent formation of a doped phase of **1**. Manual separation from the undoped **1** allowed for subsequent characterization of **$Bi_{0.97}Eu_{0.03}$-2** (Fig. S12). Elemental Analysis for $C_{31}H_{19}Bi_{0.97}Eu_{0.03}F_6N_4O_7S_2$: Calc. (Obs.): C, 39.33 (39.09); H, 2.02 (1.91); N, 5.92 (6.00 %).

[$Bi_{0.99}Eu_{0.01}Cl(TTA)_2$(terpy)] ($Bi_{0.99}Eu_{0.01}$-3)

Bismuth chloride (0.0141 grams, 0.045 mmol), TTA (0.0222 grams, 0.1 mmol), terpy (0.0112 grams, 0.05 mmol), and methanol (3 mL) were loaded into a 10 mL glass vial. The pH was increased to ca. 5-6 with 1 M potassium hydroxide in methanol (100 μL). The glass vial was capped and placed on the benchtop at room temperature. After one hour, an aliquot of 0.1 M europium chloride in methanol (50 μL, 0.005 mmol) was added to the vial. After one week, the products were filtered, washed in ethanol, and allowed to dry. Yellow blocks of **$Bi_{0.99}Eu_{0.01}$-3** were collected (Fig. S13). Yield: 39% (based on Bi). Elemental Analysis for $C_{31}H_{19}Bi_{0.99}Eu_{0.01}ClF_6N_3O_4S_2$: Calc. (Obs.): C, 40.46 (40.14); H, 2.08 (1.92); N, 4.57 (4.53 %).

[$Bi_{0.99}Eu_{0.01}Br(TTA)_2$(terpy)] ($Bi_{0.99}Eu_{0.01}$-4)

Bismuth bromide (0.020 grams, 0.045 mmol), TTA (0.0222 grams, 0.1 mmol), terpy (0.0112 grams, 0.05 mmol), and methanol (3 mL) were loaded into a 10 mL glass vial. The pH was increased to ca. 5-6 with 1 M potassium hydroxide in methanol (100μL). The glass vial was capped and placed on the benchtop at room temperature. After one hour, an aliquot of 0.1 M europium nitrate in methanol (50 μL, 0.005 mmol) was added to the vial. After one week, the products were filtered, washed in ethanol, and allowed to dry. Yellow rods of **$Bi_{0.99}Eu_{0.01}$-4** were collected (Fig. S14). Yield: 54% (based on Bi). Elemental Analysis for $C_{31}H_{19}Bi_{0.99}Eu_{0.01}BrF_6N_3O_4S_2$: Calc. (Obs.): C, 38.60 (38.41); H, 1.99 (1.88); N, 4.36 (4.40 %).

[$Bi_{0.999}Eu_{0.001}Br_2$(TTA)(terpy)] ($Bi_{0.999}Eu_{0.001}$-5)

Bismuth bromide (0.020 grams, 0.045 mmol), TTA (0.0111 grams, 0.05 mmol), terpy (0.0112 grams, 0.05 mmol), and methanol (3 mL) were loaded into a 10 mL glass vial. The pH was increased to ca. 5-6 with 1 M potassium hydroxide in methanol (100μL). The glass vial was capped and placed on the benchtop at room temperature. After one hour, an aliquot of 0.1 M europium nitrate in methanol (50 μL, 0.005 mmol) was added to the vial. After one week, the products were filtered, washed in ethanol, and allowed to dry. Yellow rods of **$Bi_{0.999}Eu_{0.001}$-5** were collected (Fig. S15). Yield: 56% (based on Bi). Elemental Analysis for $C_{23}H_{15}Bi_{0.999}Eu_{0.001}Br_2F_3N_3O_2S$: Calc. (Obs.): C, 33.51 (33.38); H, 1.96 (1.74); N, 5.09 (5.05 %).

Single crystal X-ray diffraction

Single crystals of **1 - 6** were selected from the bulk sample and mounted on MiTeGen micromounts in N-paratone. Single crystal X-ray diffraction data were collected at 100(2) K on a Bruker D8 Quest diffractometer equipped with an I*u*S X-ray source (Mo-Kα radiation; λ=0.71073 Å) and a Photon 100 CMOS detector. Data were integrated using the SAINT software package included with APEX2.[50, 51] An absorption correction was applied using a multi-scan technique in SADABS.[52] The structures were solved using direct methods via SHELXT and refined by full-matrix least-squares on F2 using the SHELXL software in shelXle64.[53, 54] Crystallographic data for compounds **1 - 6** are provided in Table 1, and the resulting CIF data are available as Supporting Information. Crystallographic data were deposited in the Cambridge Crystallographic Date Centre (CCDC) and may be found at http://www.ccdc.cam.ac.uk/ by using reference numbers 1913266 – 1913271.

Table 1. Crystallographic Structure Refinement Details for compounds **1 - 6**.

	1	**2**	**3**	**4**	**5**	**6**
Formula	$C_{32}H_{28}Bi_2N_{10}O_{14}$	$C_{31}H_{19}BiF_6N_4O_7S_2$	$C_{31}H_{19}BiClF_6N_3O_4S_2$	$C_{31}H_{19}BiBrF_6N_3O_4S_2$	$C_{23}H_{15}BiBr_2F_3N_3O_2S$	$C_{31}H_{19}EuF_6N_4O_7S_2$
MW ($gmol^{-1}$)	1194.60	946.60	920.05	964.50	823.23	889.59
T (K)	100(2)	100(2)	100(2)	100(2)	100(2)	100(2)

λ (K α)	0.71073	0.71073	0.71073	0.71073	0.71073	0.71073
μ (mm^{-1})	9.944	5.654	5.958	7.11	10.54	2.114
Crystal System	Monoclinic	Monoclinic	Triclinic	Triclinic	Monoclinic	Monoclinic
Space Group	$P2_1/n$	$C2/c$	$P\text{-}1$	$P\text{-}1$	$C2/c$	$C2/c$
a (Å)	11.0626(5)	36.9106(21)	10.3216(5)	10.2659(6)	30.2542(14)	37.6364(16)
b (Å)	13.5522(6)	9.7235(6)	10.7535(5)	10.8192(6)	8.7876(4)	9.6744(4)
c (Å)	11.9227(5)	17.9854(11)	14.8647(7)	14.9442(8)	18.6371(8)	18.2345(7)
α (°)	90	90	91.665(2)	91.545(2)	90	90
β (°)	94.194(2)	90.197(2)	91.689(2)	92.281(2)	96.051(1)	95.909(1)
γ (°)	90	90	109.018(2)	109.003(2)	90	90
Volume ($Å^3$)	1782.70(14)	6487.1(5)	1557.84(13)	1566.73(15)	4926.8(4)	6604.1(5)
Z	2	8	2	2	8	8
R_{int}	0.0668	0.0919	0.0445	0.0311	0.0371	0.0365
R ($I > 2\sigma$)	0.0277	0.0409	0.0207	0.0144	0.0185	0.0275
wR_2	0.0461	0.0839	0.0393	0.0338	0.0425	0.0652
GooF	1.021	1.024	1.027	1.052	1.128	1.061
Residual density (max/min)	2.30/-0.75	1.62/-0.69	0.98/-0.76	1.18/-0.61	0.67/-1.06	1.44/-0.67
CCDC No.	1913266	1913267	1913269	1913270	1913268	1913271

Characterization methods

Powder X-ray diffraction data were collected for the bulk samples from which single crystals of **1** – **6** were isolated using Cu-Kα radiation (λ = 1.542 Å) on a Rigaku Ultima IV X-ray diffractometer from 3-40˚ in 2θ with a step speed of 1 degree/min. Raman spectra were collected for single crystals selected from the bulk using an excitation source of 532 nm (maximum power = 100 mW) on a Horiba LabRAM HR Evolution Raman Spectrometer. Spectra were recorded from 200 to 2000 cm^{-1} with 10 accumulations and a laser power between 5 and 10% (Figs. S16-S21). Combustion elemental analysis was carried out using a Perkin Elmer Model 2400 Elemental Analyzer on the manually separated bulk phases. Thermogravimetric analyses were conducted on the manually separated bulk sample using a TA Instruments Q50 Thermogravimetric Analyzer under flowing N_2 (flow rate = 10 mL/min) from 30 to 600 °C with a step speed of 5 °C/min. Inductively coupled plasma-mass spectrometry was collected on an Agilent 7700 ICP-

MS to determine bismuth:europium ratios. A calibration curve was made for both Bi and Eu using 10 different concentrations (5, 7.5, 10, 50, 100, 500, 1000, 1500, and 2000 ppb); all solutions were made using 5% HNO_3. Roughly 5 mg of each sample was dissolved in 5% HNO_3 under slight heating and stirring and diluted to within the calibration curve range. Reported doping percentages are the average of multiple samples.

Photoluminescence measurements

Luminescent measurements were performed on a Horiba PTI QM-400 system (Horiba PTI) on solid samples at room temperature. The samples were placed between two glass slides and collected using fluorimeter slit widths of 1–3 nm. Harmonic oscillations from the excitation source were blocked using long-pass filters (455 or 495 nm). In all cases, the wavelength of the peak of maximum intensity in the excitation spectrum was used to generate the emission spectrum. Time-resolved measurements were collected using a Xenon flash lamp as the average of 10,000 shots. Quantum yield measurements were acquired using an 8.9 cm integrating sphere coated in Spectralon fluoropolymer. Samples were ground into homogenous powders in dried potassium bromide (KBr) using a 1:50 sample:KBr ratio and then loaded into a Teflon sample holder placed within the sphere at a 45° angle to the incident beam. The quantum yield of anthracene was determined concurrently against the Eu-containing samples to ensure validity of the quantum yield. Reported lifetimes and quantum yields are the average of three collections.

Singlet and triplet states of TTA and terpy were determined by dissolving $Gd(NO_3)_3 \cdot 6H_2O$ (0.077 mmol, 0.034 g) and TTA (0.231 mmol, 0.051 g) or terpy (0.231 mmol, 0.054 g) in 5 mL of a 1:1 MeOH–EtOH mixture in a 10 mL glass vial. The solution was gently heated to 50 °C to ensure complete dissolution of all chemicals. An aliquot of each solution was introduced into an NMR tube for low temperature collection. Measurements were taken on a Horiba PTI QM-400 system equipped with a liquid nitrogen dewar assembly and a pulsed-UV xenon flash lamp at 77 K. Spectra were first recorded using a time delay of 0.1 ms to avoid lamp flash, a sample window of 1 ms, and 20 pulsed flashes to resolve both fluorescence and phosphorescence emission peaks. Next, using a time delay of 0.5 ms to remove any residual fluorescence, phosphorescence of the Gd-ligand complexes was observed with a sample window of 1 ms and 20 pulsed flashes. All emission spectra were collected with a slit width of 5 nm for both excitation and emission monochromators with an excitation wavelength of 325 nm, and are uncorrected. The spectra can be found in the supporting information (Figs. S43-44).

RESULTS

Synthesis

Various metal:ligand ratios were explored for the synthesis of each compound in order to examine any structural variation that may arise from reaction conditions. With $Bi(NO_3)_3$ or $BiCl_3$ as the bismuth precursor, only the X-Bi structural motif was observed with a Bi:TTA:terpy ratio range of 1:1:1 to 1:2:2. With $BiBr_3$, a change in the reaction product was observed by changing the Bi:TTA:terpy ratio. At a 1:1:1 ratio, the Br-Bi-Br structural motif was observed (**5**), whereas a 1:2:1 ratio yielded the Br-Bi motif (**4**). The bond dissociation for Bi-Br is higher than that of Bi-O and Bi-Cl, so formation of both **4** and **5** is not unexpected.[55] Synthesis of the europium doped analogs were attempted using synthetic conditions identical to those used to prepare the homometallic phases. This approach was only successful for **6**, possibly due to differences in solubility between the bismuth and europium salt precursors.

Differences in the solubility of the bismuth- and europium salts as well as differing reaction kinetics led to challenges in preparing lanthanide doped samples of **2** – **5**. Initially, in an effort to keep the counter-anion identical upon addition of Eu^{3+}, $Eu(NO_3)_3$, $EuCl_3$, and $EuBr_3$ solutions were added to the respective reaction vials to prepare **2** - **5**. However, this approach was only successful for **2** and **3** when $Eu(NO_3)_3$ and $EuCl_3$ were added immediately and after one hour, respectively. Due to the rapid formation of **2**, the europium nitrate aliquot was added immediately following addition of the solvent. Addition of europium nitrate after >15 minutes resulted in a distinct absence of europium incorporation in **2** based on visual inspection as the majority of the product had likely already formed. The undoped compound **2** forms significantly faster than **6**, further highlighting the differences in reaction kinetics between the Bi-TTA/terpy and Eu-TTA/terpy phases. For **3**, doping was possible with both $Eu(NO_3)_3$ and $EuCl_3$, but only characterization of the phase doped with $EuCl_3$ is reported herein. For **4** and **5**, addition of $EuBr_3$ as the europium salt did not lead to successful incorporation of europium into the bismuth host materials, irrespective of when the europium bromide was added to the solution. We attribute this to the differences in solubility of the europium nitrate and bromide salts under the given reaction conditions, i.e. the nitrate

salt is more soluble in methanol. Thus, $Eu(NO_3)_3$ was added to the reaction vial of **4** and **5** an hour after the initial reaction began to yield $\mathbf{Bi_{0.999}Eu_{0.001}}$**-5**. Addition of a europium nitrate aliquot at the start of the reaction resulted in no Eu incorporation into the crystalline product based on visual inspection. We have made use of similar doping strategies in lanthanide-doped bismuth-thiophenedicarboxylates, where a lanthanide salt aliquot was added to the reaction vial a day after the start of the reaction.[23]

Structure descriptions

$[Bi_2(terpy)_2(MeO)_2(NO_3)_4]$ (1)

The asymmetric unit of **1** consists of one Bi^{3+} metal center, two nitrate ions, one methoxy group, and one κ^3-terpy ligand. Each bismuth is nine-coordinate, bound to four O atoms from two bidentate nitrate ions, two O atoms from two bridging methoxy groups, and three N atoms from one terpy. The bismuth adopts a

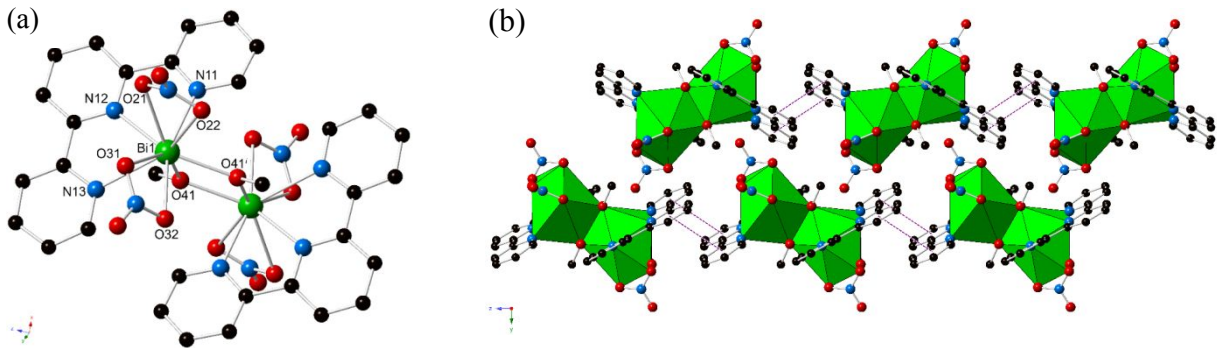

distorted tricapped trigonal prismatic coordination geometry. The Bi-O distances range from 2.663(3) to 2.734(3) Å for the nitrates and 2.225(3) to 2.375(3) Å for the bridging O atoms from the methoxy. The Bi-$O_{methoxy}$ distances fall within expected distances for a bridging methoxy group rather than a singly bound methanol.[56, 57] The Bi-N distances range from 2.402(4) to 2.585(4) Å. Bi1 is bridged to a second bismuth center through two O atoms from two methoxy groups to form discrete dimeric units (Fig. 1a). Intermolecular interactions including H-bonding and π-π stacking were examined using Platon.[58] No classic hydrogen bonding interactions were found; however, evidence of C-H ··· O hydrogen bonding are present. [59, 60] Relevant C-H ··· Acceptor distances and angles are provide in Table S1.Weak, offset π-π stacking is observed between terpyridine ligands of adjacent dimeric units with $C_{terpy}\cdots C_{terpy}$ = 3.969(3) Å and the slip angle = 28.0˚. This π-π stacking interactions bridge the dimers into supramolecular 1D chains along the [001] as illustrated in Fig. 1b.

Fig. 1 (a) Illustration of the dimeric unit in **1**. (b) Packing diagram of **1** viewed down the [100] depicting π-π stacking interactions (purple dashed lines) between terpy ligands from adjacent dimers. Green polyhedra are nine coordinate BiO_6N_3. Green, red, blue, and black spheres are bismuth, oxygen, nitrogen, and carbon atoms, respectively. Hydrogen atoms have been omitted for clarity.

$BiNO_3(TTA)_2$(terpy) (2)

The asymmetric unit of **2** is comprised of one Bi^{3+} metal center, one κ^2-nitrate, two κ^2-TTA ligands, and one κ^3-terpy ligand. As shown in Fig. 2, the bismuth is nine-coordinate, adopting a distorted monocapped square antiprismatic coordination geometry. The Bi^{3+} metal center is bound to four O atoms from two TTA ligands, two O atoms from one nitrate, and three N atoms from one terpy. The Bi-O distances range from 2.318(5) to 2.539(4) Å for the TTA and are 2.626(4) and 2.711(4) Å for the O atoms from the nitrate. The Bi-N distances range from 2.518(5) to 2.555(5) Å. Intermolecular π-π stacking interactions are observed between adjacent aromatic rings, as shown in Fig. 2b, and bridge the monomeric units into supramolecular 2D sheets along the xz plane. These interactions occur between adjacent terpy ligands with $C_{terpy}\cdots C_{terpy}$ = 3.669(4) Å, slip angle = 22.0˚ and between one disordered thiophene and an adjacent terpy ligand, $C_{thiophene}\cdots C_{terpy}$ = 3.779(8) Å, slip angle = 20.5˚ for Part A. No classic hydrogen bonding interactions were found;[59, 60] C-H ··· Acceptor distances and angles are provide in Table S2.

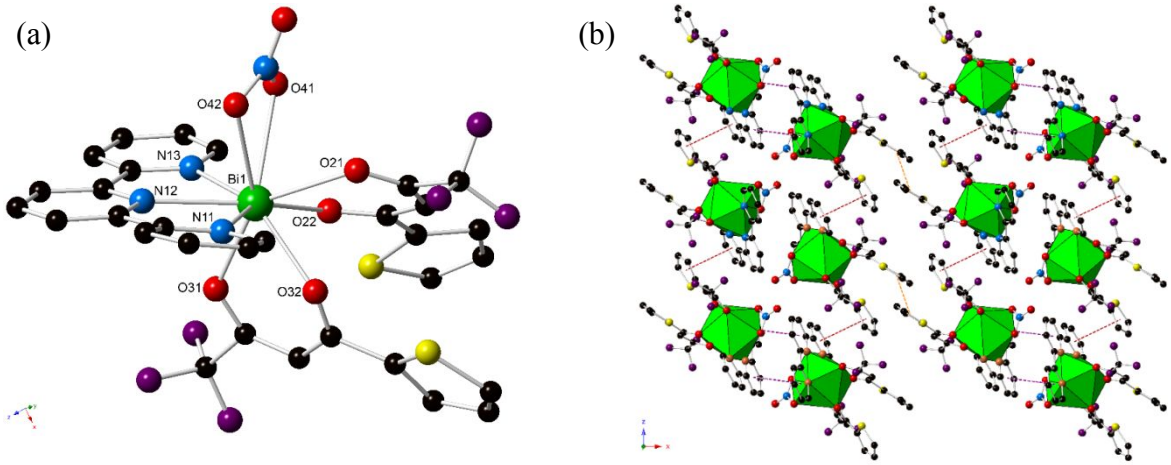

Fig. 2 (a) Illustration of the monomeric unit in **2**. (b) Polyhedral representation of the packing diagram of **2** viewed down the [010] depicting π-π stacking interactions including thiophene···terpy (red dashed lines), terpy···terpy (purple dashed lines), and thiophene-thiophene (orange dashed lined). Green polyhedra are nine coordinate BiO_6N_3. Green, red, purple, yellow, blue, and black spheres are bismuth, oxygen, fluorine, sulfur, nitrogen, and carbon atoms, respectively. Hydrogen atoms and disorder of the thiophene rings have been omitted for clarity.

$BiCl(TTA)_2$(terpy) (3)

The asymmetric unit of **3** consists of one Bi^{3+} atom, one Cl atom, two κ^2-TTA ligands, and one κ^3-terpy ligand. The Bi^{3+} is eight-coordinate, forming a distorted bicapped trigonal prismatic coordination geometry. The bismuth metal center is bound to one Cl atom, four O atoms from two TTA ligands, and three N atoms from one terpy ligand (Fig. 3a). The Bi-Cl bond distance is 2.5879(8) Å and the Bi-O and Bi-N distances range from 2.420(2) to 2.641(2) Å and 2.508(2) to 2.530(2) Å, respectively. The monomeric units are bridged into supramolecular 2D sheets along the xz plane via π-π stacking interactions (Fig. 3b). The thiophene ring of one TTA and the two peripheral rings of the terpy display moderately strong π-π interactions ($C_{thiophene}\cdots C_{terpy}$ = 3.571(2) Å, slip angle = 18.3˚; $C_{thiophene}\cdots C_{terpy}$ = 3.474(3) Å, slip angle = 18.4˚). The thiophene ring of one TTA displays π-π interactions to a symmetry equivalent thiophene ring of an adjacent TTA ligand with the distances between centroids and the slip angles equal to 3.599(7) Å, 21.6˚ and 3.655(8) Å, 21.9˚ for Part A. Additionally, each Bi-bound terpy ligand interacts with a terpy from an adjacent complex, with the closest $C_{terpy}\cdots C_{terpy}$ distance = 3.647(2) Å and the slip angle = 21.2˚. Evidence of a halogen-π interaction is observed between Cl1 and the center of a pyridine ring (N32), where $Cl1\cdots C_{terpy}$ = 4.271(4) Å with α = 34˚ corresponding to the angle between the vector along the terpy centroid-Cl1 line and the vector normal to the plane in which the terpy ring lies.[61, 62] No classic hydrogen bonding interactions were found;[59, 60] C-H ··· Acceptor distances and angles are provide in Table S3.

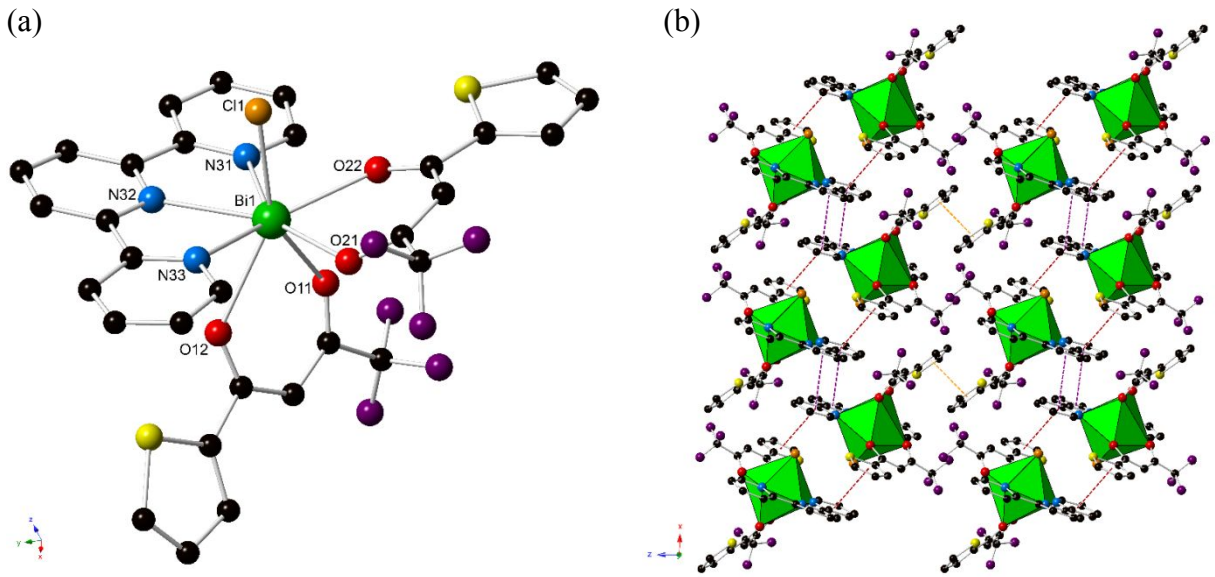

Fig. 3 (a) Illustration of the monomeric unit in **3**. (b) Packing diagram of **3** viewed down the [010] depicting π-π stacking interactions including thiophene···terpy (red dashed lines), terpy···terpy (purple dashed lines), and thiophene-thiophene (orange dashed lines). Green polyhedra are eight coordinate $BiClO_4N_3$. Green, red, purple, yellow, blue, orange, and black spheres are bismuth, oxygen, fluorine, sulfur, nitrogen, chlorine, and carbon atoms, respectively. Hydrogen atoms and disorder of the thiophene rings have been omitted for clarity.

$BiBr(TTA)_2$(terpy) (4)

Compound **4** is isomorphous to **3**; the asymmetric unit consists of one Bi^{3+} atom, one Br atom, two κ^2-TTA ligands, and one κ^3-terpy ligand. The bismuth is eight-coordinate, forming a distorted bicapped trigonal prismatic coordination geometry. Each Bi^{3+} metal center is bound to one Br atom, four O atoms from the TTA ligands, and three N atoms from the terpy ligand. The Bi-Br distance is 2.748(2) Å, the Bi-O distances range from 2.461(3) to 2.613(3) Å, and the Bi-N distances range 2.510(3) from to 2.434(3) Å. As in **3**, π-π stacking interactions yield supramolecular 2D sheets that extend along the xz plane. Interactions are observed between the thiophene ring of one TTA and the outer rings of the terpy ($C_{thiophene}\cdots C_{terpy}$ =

3.4923(2) Å, slip angle = 18.8˚; $C_{thiophene}\cdots C_{terpy}$ = 3.5979(2) Å, slip angle = 18.2˚). Further, the thiophene ring of one TTA displays π-π stacking interactions to a symmetry equivalent thiophene ring of an adjacent TTA ligand with the distances between centroids and the slip angle equal to 3.6019(2) Å and 21.4˚, respectively, for Part A. Finally, the terpy ligand stacks with additional terpy ligands in adjacent monomeric units, with the closest $C_{terpy}\cdots C_{terpy}$ distance of 3.6273(2) Å and slip angle of 21.7˚. As observed in **3**, a halogen-π interaction is observed between Br1 and the center of the pyridine ring of terpy; $Br1\cdots C_{terpy}$ = 4.213(4) Å with α = 36˚. C-H ··· Acceptor distances and angles are provide in Table S4.

$BiBr_2$(TTA)(terpy) (5)

Compound **5** is composed of one unique Bi^{3+} metal center, two Br atoms, one κ^2-TTA ligand, and one κ^3-terpy ligand. The bismuth center is seven-coordinate, bound to two Br atoms, two O atoms from the TTA, and three N atoms from the terpy, forming discrete monomeric units (Fig. 4a). The bismuth cation adopts a slightly distorted pentagonal bipyramidal coordination geometry with Br1-Bi1-Br2 angle = 173.2˚. The Bi-Br, Bi-O, and Bi-N distances are 2.753(1) and 2.911(1) Å, 2.417(2) and 2.465(2) Å, and 2.512(3) - 2.525(3) Å, respectively. Each monomer interacts with two other monomeric units via π-π stacking interactions between the thiophene ring of the TTA and terpy ($C_{thiophene}\cdots C_{terpy}$ = 3.8346(2) Å, slip angle =

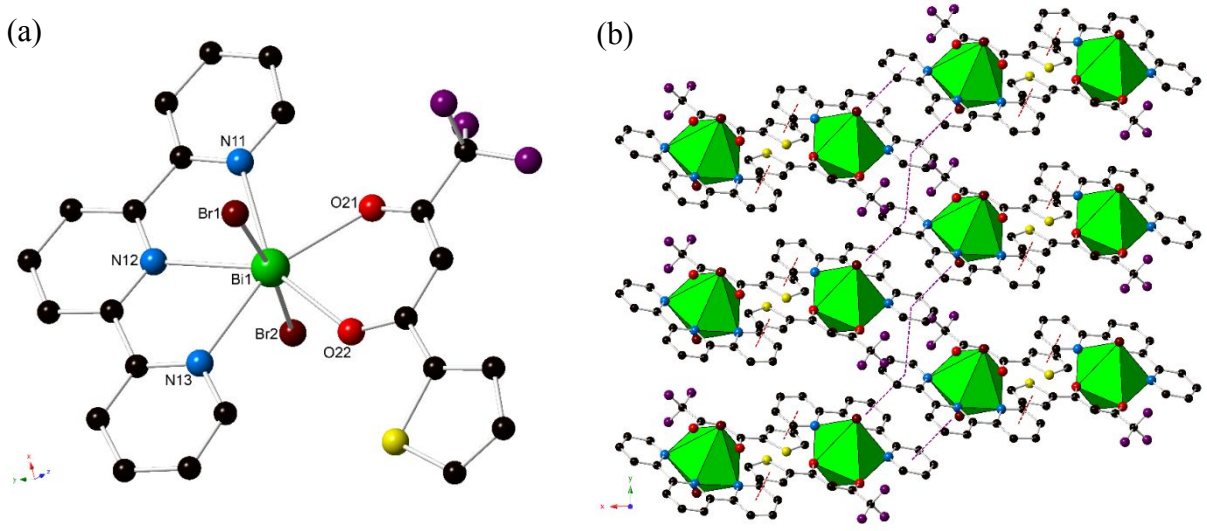

21.9˚) and between adjacent terpy ligands ($C_{terpy}\cdots C_{terpy}$ = 3.6545(2) Å, slip angle = 20.6˚ and 3.874(2)). These intermolecular interactions bridge the monomers into supramolecular 2D sheets in the xy plane as shown in Fig. 4b. C-H ··· Acceptor distances and angles are provide in Table S5.

Fig. 4 (a) Illustration of the monomeric unit in **5**. Green, red, purple, yellow, blue, dark red, and black spheres are bismuth, oxygen, fluorine, sulfur, nitrogen, bromine, and carbon atoms, respectively. Hydrogen atoms have been omitted for clarity. (b) Packing diagram of **5** viewed down the [010] depicting π-π interactions including thiophene···terpy (red dashed lines) and the terpy···terpy ligands (purple dashed lines) interactions. Green polyhedra are seven coordinate $BiBr_2O_2N_3$. Green, red, purple, yellow, blue, dark red, and black spheres are bismuth, oxygen, fluorine, sulfur, nitrogen, bromine, and carbon atoms, respectively. Hydrogen atoms have been omitted for clarity.

$EuNO_3(TTA)_2$(terpy)·0.3MeOH (6)

Compound **6** is built from one crystallographically unique Eu^{3+} metal center, one κ^2-nitrate, two κ^2-TTA ligands, and one κ^3-terpy ligand (Fig. 5). The complex is isostructural to the bismuth complex in **2**. The europium is nine-coordinate, forming a distorted monocapped square antiprismatic coordination geometry. Each Eu^{3+} center is bound to four O atoms from the TTA ligands, two O atoms from the nitrate, and three N atoms from the terpy. The Eu-O distances range from 2.348(3) to 2.408(3) Å for the TTA. The nitrate Eu-O bond distances are 2.521(3) to 2.567(3) Å. The Eu-N distances range from 2.542(4) to 2.577(4) Å. A

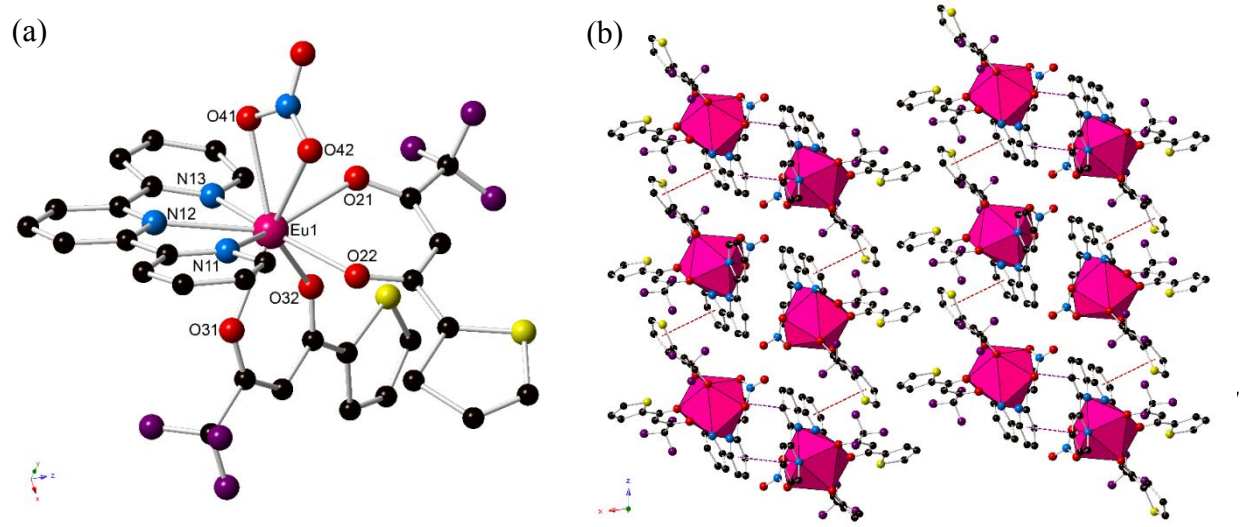

partially occupied (~30%) methanol is located in the outer coordination sphere. The compound consists of monomeric units that display similar intermolecular interactions to that of **2**. Displaced parallel π-π stacking interactions are observed between adjacent terpy ligands with $C_{terpy}\cdots C_{terpy}$ = 3.638(2) Å and a slip angle = 19.9˚. There are also weak stacking interactions between the one disordered thiophene and an adjacent terpy, $C_{thiophene}\cdots C_{terpy}$ = 3.828(12) Å, slip angle = 23.1˚ for Part A as shown in Fig. 5b. No classic hydrogen bonding interactions were found;[59, 60] C-H ··· Acceptor distances and angles are provide in Table S2.

Fig. 5 (a) Illustration of the monomeric unit in **6**. (b) Packing diagram of **6** viewed down the [010] depicting π-π interactions including thiophene···terpy (red dashed lines) and the terpy···terpy (purple dashed lines). Pink polyhedra are nine coordinate EuO_6N_3. Pink, red, purple, yellow, blue, and black spheres are europium, oxygen, fluorine, sulfur, nitrogen, and carbon atoms, respectively. Hydrogen atoms have been omitted for clarity.

Raman spectroscopy

Raman spectra were collected for single crystals of **1 - 6** (Figs. S17-22). The spectrum for each compound showed characteristic ligand peaks, and for **3 – 5**, Bi-X (X=Cl, Br) vibrations were observed. The peaks between 200-315 cm^{-1} can be attributed to ν(Bi-X) vibrations in **3 – 5**.[63, 64] The peaks observed between 1000 and 1700 cm^{-1} are attributed to overlapping bands from C-H, $C-F_3$, C-O, C-N, and ring vibrations from the thienyl and/or terpyridine groups.[65]

Thermal analysis

The thermal stability of **2 – 6** was examined over 30 °C to 600 °C under flowing nitrogen and powder X-ray diffraction data were collected to identify the thermal decomposition products. Each phase shows good thermal stability up to >150 °C. For **2**, decomposition occurred over one step (Fig. S22). Decomposition begins around 150 °C and was complete just past 400 °C. The total weight loss (72.7 %) along with the

PXRD data (Fig. S27) were consistent with decomposition to Bi_2O_3 (calc. 75.4%); however, several peaks in the powder pattern could not be accounted for by Bi_2O_3.[66] The thermal decomposition of **3** occurred over three consecutive steps (Fig. S23). The first weight loss (18%) began around 150 °C and is attributed to loss of one TTA ligand (calc. 20.0%). A second weight loss (42%) began immediately following the first at around 200 °C and may be attributed to lose of the second TTA ligand and terpy (calc. 39.5%). The final weight loss of 11% began at about 325 °C and concluded just past 475 °C. The overall weight loss is consistent with decomposition to the "Arppe Compound" $Bi_{24}O_{31}Cl_{10}$ (calc. 73.4%, obs. 70.5%) and is supported by the powder pattern collected on the decomposition product (Fig. S28).[67] The thermal decomposition of **4** had an overall weight loss of 75.8% over four consecutive steps (Fig. S24). The first weight loss (21.4%) began around 175 °C and is consistent with loss of a TTA ligand (calc. 19.6%). Immediately thereafter, the second weight loss (37.7%) began at 230 °C and is attributed to loss of the second TTA ligand and terpy (calc. 39.4%). The third weight loss of 10% began at ca. 350 °C and was complete at 470 °C. The final weight loss (6.7%) was complete just before 600 °C. PXRD data of the thermal product indexes to $Bi_{24}O_{31}Br_{10}$ (calc. 72.8%) (Fig. S29). The thermal decomposition of **5** had an overall weight loss of 68.6% over two consecutive drops (Fig. S25). The first weight loss (64.1%) began around 150 °C and was complete by 350 °C. The second and final weight loss of 4.6% was complete by 460 °C. PXRD data collected for the thermal decomposition product indexes to $Bi_{24}O_{31}Br_{10}$ (calc. 68.1%) (Fig. S30). The thermal decomposition of **6** had an overall weight loss of 72.9% over three consecutive drops (Fig. S26). The first weight loss (58.4%) began around 200 °C and was complete at 325 °C, at which time the second weight loss (5.7%) began. These two drops are consistent with loss of both TTA ligands and terpy (calc. 64.1%). The final weight loss (9%) began at 400 °C and concluded just before 600 °C. PXRD data of the thermal product did not index to any reported europium-inorganic phases (Fig. S31).

Doping Studies

Successful doping of europium into each bismuth compound was confirmed by powder XRD, ICP-MS, and luminescence/lifetime data. Further inspection of the crystal structure shows maximum void diameters less than 4.9 Å in each case, indicating that a hydrated europium ion (diameter = ~4.9 Å) is unlikely to reside in any open volume.[68] Phase separation was prevented by careful introduction of the europium salt to the reaction vial prior to crystallization of the bismuth phase as outlined above. Powder patterns of each doped phase are in good agreement with the calculated pattern of the corresponding homometallic phase, consistent with Eu incorporation into the bismuth phase (Figs. S12-15). The ratio of europium doped into each bismuth compound was determined through ICP-MS. The percentages of europium incorporation are shown in Table 2 and are the average of three separate preparations. The given percentages reflect the maximum doping levels achieved even at doping levels up to 10% in the synthesis. All show limited doping. Compound **2** displays the highest doping level (2.9%) of the four compounds, which could be due to the isostructural nature of the complexes in **2** and **6**. Yet it is worth noting that despite the similarities in the local coordination environments of the Bi- and Eu- metal centers in **2** and **6**, we were not able to prepare solid-solutions. This may point to the importance of not only controlling the coordination chemistry of Bi- and Eu- but also the relative solubility of the complexes, such that higher doping levels may be achieved. Perhaps unsurprisingly, **5** shows the lowest amount of Eu incorporation, possibly attributed to the presence of two bromide ions bound to the metal center. In contrast to europium chloride-organic compounds, few europium bromide-organic compounds have been reported. The Eu-Br structural motif is relatively uncommon and the Br-Eu-Br motif even more so. Thus, the low europium doping in **5** likely results from

the unfavorable (for Eu) metal ion coordination environment, with two soft bromide ions.[69] This is supported by our inability to obtain europium analogs of **4** and **5**.

Table 2. Percent ion doping into each compound.

	Eu Doping (mol%)
$Bi_{0.97}Eu_{0.03}$-2	2.9 ± 0.5
$Bi_{0.99}Eu_{0.01}$-3	1.2 ± 0.3
$Bi_{0.99}Eu_{0.01}$-4	1.4 ± 0.2
$Bi_{0.999}Eu_{0.001}$-5	0.06 ± 0.01

Luminescent Behavior

The room temperature emission spectra of the free ligands, TTA and terpy, were collected for reference and showed weak emission peaks centered at 449 and 373 nm, respectively (Figs. S32-S33). This emission likely results from intra-ligand $\pi \rightarrow \pi^*$ and/or $n \rightarrow \pi^*$ transitions. The singlet and triplet states of the ligands were determined through time-delayed measurements at 77 K using the respective Gd-ligand complex in solution. These values are provided in Table 3. They are in good agreement with literature values of the singlet and triplet excited states.[70] The emission spectra of the gadolinium complex with both TTA and terpy present shows emission of the TTA ligand only. This is consistent with the relative energy levels of the excited states for both ligands, where TTA lies lower in energy than terpy; its triplet state could reasonably be populated via energy transfer from the excited states of terpy.

Table 3. Singlet and triplet states of the ligands.

	Singlet (cm^{-1})	Triplet (cm^{-1})
Gd-TTA	26,738	21,505
Gd-terpy	28,011	22,988

The bismuth-only compounds appear non-luminescent at room temperature when irradiated with a handlamp. However, each phase displays notably weak ligand luminescence with broad emission bands ranging from ca. 350 to 550 nm when excited between 315-327 nm (Figs. S34-S37). Broad emission from TTA and terpy are observed in **2** with a λ_{max} at 380 nm. Compounds **3** and **4** show distinct terpy and TTA emission at ~375 and ~446 nm, respectively, and also show peaks centered at ca. 500 nm. Compound **5**

likewise displays emission bands consistent with terpy and TTA, and a much stronger band centered at 520 nm.

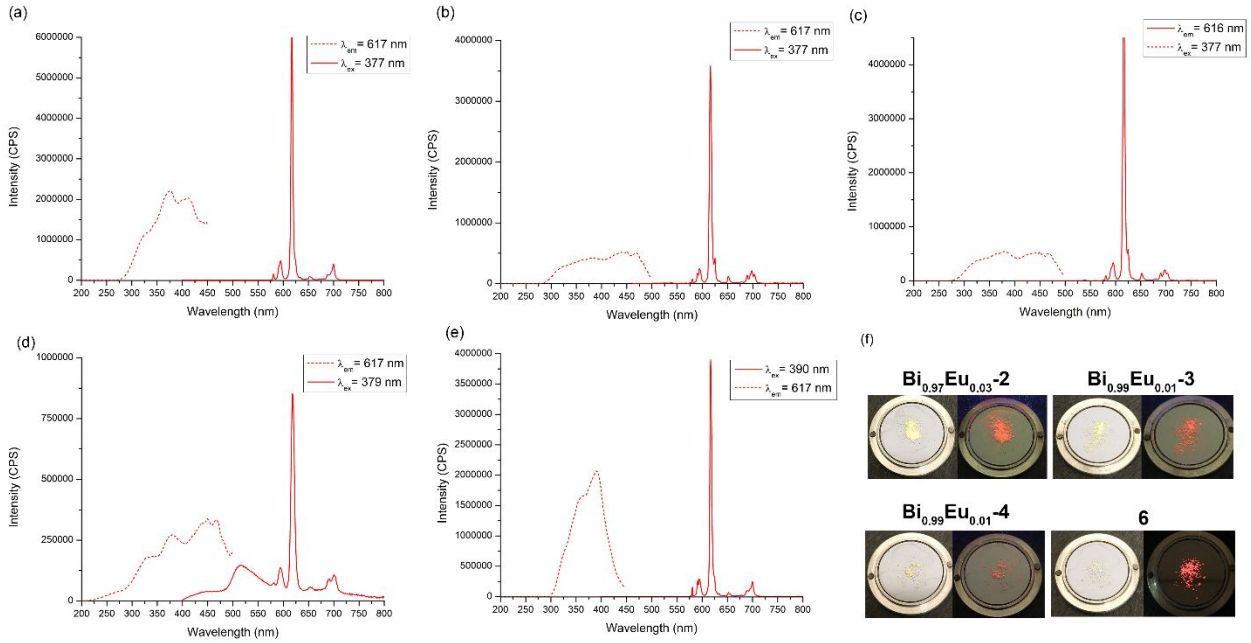

Fig. 6 Room temperature excitation (dashed line) and emission (solid line) spectra of (a) **$Bi_{0.97}Eu_{0.03}$-2,** (b) **$Bi_{0.99}Eu_{0.01}$-3**, (c) **$Bi_{0.99}Eu_{0.01}$-4**, (d) **$Bi_{0.999}Eu_{0.001}$-5** and (e) **6**, and images (f) of the bulk compounds under ambient light (left) and UV light (right). An image is not displayed for **$Bi_{0.999}Eu_{0.001}$-5** as emission is not noticeable to the naked eye, most likely due to the low doping amount.

The room temperature solid-state luminescence spectra of the europium-doped compounds were measured; all displayed Eu-based emission in the visible region. While the quantum yield for **$Bi_{0.97}Eu_{0.03}$-2** was approximately 5%, that of the remaining Eu doped compounds was below 1%. A broad excitation spectrum was observed for **$Bi_{0.97}Eu_{0.03}$-2** centered at 420 nm. Excitation at this wavelength yielded red luminescence characteristic of europium (Fig. 6a). The peaks at 594 and 617 nm are assigned to the $^5D_0 \rightarrow {}^7F_J$ (J = 1, 2), while the $^5D_0 \rightarrow {}^7F_0$ transition is observed at 580 nm. Peaks centered at 652 and 699 nm can be assigned to the $^5D_0 \rightarrow {}^7F_J$ (J = 3, 4) transitions, respectively. Time resolved measurements of the $^5D_0 \rightarrow {}^7F_2$ transition gave a lifetime of 664(44) μs (Fig. S38). Quantum yield measurements yielded a quantum yield of 0.052(9).

For **$Bi_{0.99}Eu_{0.01}$-3**, the excitation maximum was centered at 451 nm (Fig. 6b). The $^5D_0 \rightarrow {}^7F_J$ (J = 0 - 2) transitions were observed at 580, 594, and 617 nm, respectively. Broad, weak peaks centered around

651 and 698 nm can be assigned to the $^5D_0 \rightarrow {}^7F_J$ (J = 3, 4) transitions, respectively. The compound possesses an emissive lifetime of 506(1) μs (Fig. S39).

$Bi_{0.99}Eu_{0.01}$-4 displays characteristic red luminescence when excited at a wavelength of 377 nm (Fig. 6c). The $^5D_0 \rightarrow {}^7F_J$ (J = 0 - 3) transitions are observed at 581, 595, 616, and 652 nm respectively, while the broad peak centered at 698 nm can be assigned to the $^5D_0 \rightarrow {}^7F_4$ transition. The emissive lifetime was found to be 547(4) μs (Fig. S40).

The excitation spectrum for **$Bi_{0.999}Eu_{0.001}$-5** (Fig. 6d) showed a peak maximum at 382 nm. Excitation at this wavelength gave an emission spectrum with a broad ligand emission centered at 520 nm; this feature is similar to the ligand-based emission seen in the undoped **5**. We attribute this peak to TTA emission, based on the triplet states determined for TTA and terpy. The $^5D_0 \rightarrow {}^7F_J$ (J = 1, 2) transitions are assigned to the emission peaks at 594 and 617 nm, respectively, while the $^5D_0 \rightarrow {}^7F_0$ transition is at 580 nm. Broad, weak peaks centered around 654 and 700 nm can be assigned to the $^5D_0 \rightarrow {}^7F_J$ (J = 3, 4) transitions, respectively. The fluorescence lifetime of **$Bi_{0.999}Eu_{0.001}$-5** was 469(5) μs (Fig. S41).

A broad excitation maximum centered at 390 nm was observed for **6** (Fig. 6e). Excitation at this wavelength gave an emission spectrum with well-defined $^5D_0 \rightarrow {}^7F_J$ (J = 1, 2) transitions at 594 and 617 nm, respectively. The peak at 581 nm is attributed to the $^5D_0 \rightarrow {}^7F_0$ transition. Broad, weak peaks centered around 652 and 700 nm can be assigned to the $^5D_0 \rightarrow {}^7F_J$ (J = 3, 4) transitions, respectively. The fluorescence lifetime and quantum yield of **6** were determined to be 623(39) μs (Fig. S42) and 0.146(12), respectively.

Table 4. Photophysical measurements for **$Bi_{0.97}Eu_{0.03}$-2** and **Eu-6.** The quantum yields of **$Bi_{0.99}Eu_{0.01}$-3**, **$Bi_{0.99}Eu_{0.01}$-4**, and **$Bi_{0.999}Eu_{0.001}$-5** were less than 1%.

	φ_{tot}	φ_{Eu}	Lifetime (μs)	η_{sens}
$Bi_{0.97}Eu_{0.03}$-2	0.052(9)	0.44	664(44)	0.12
Eu-6	0.146(12)	0.39	623(39)	0.37

DISCUSSION

There are approximately seven unique bismuth-terpy phases[9, 71-74] and no bismuth-TTA compounds reported in the CSD. Of the Bi-terpy phases reported four contain bound iodide and one has bound chloride; none consist of bromide. Expansion of the search to include structures with a Bi-X_1 structural motif (X=Cl or Br) results in approximately 234 compounds wherein only one halide is bound to the metal center as observed in **2** and **3**. Few of those exhibit an eight-coordinate metal center, highlighting the relative scarcity of this structural motif for Bi-organic compounds. For comparison, a search for structures with a Bi-X_2 motif (X=Cl or Br, with two halides bound to the metal center) yielded nearly 200 results. Approximately ten of those consisted of seven-coordinate metal centers like those observed in **4**. It is perhaps surprising then that we only saw formation of **4** upon changing metal:ligand ratios and no formation of its chloride analog. Further, compound **1** is isostructural to a previously reported bismuth-terpy dimer reported by Junk et al., $Bi_2(terpy)_2(OH)_2(NO_3)_4$, in which the bismuth centers are instead bridged through two hydroxides.[71] This is only the second example of a Bi-(μ-MeO)$_2$-Bi structural motif, and the first example wherein the methoxy originates from an *in situ* reaction rather than a methoxy precursor as reported by Yin et al.[56] The methoxy bridging group in **1** must come from the methanol in the reaction.

Trivalent bismuth is an ns^2 metal center and often portrays a degree of asymmetry in its coordination sphere that can be attributed to the presence of the structure directing $6s^2$ lone pair. Both an open face and clear asymmetry in the Bi-O bond lengths are evidence of a stereochemically active lone pair. [23, 75] This bond asymmetry is notably absent in the complexes presented here suggesting that the lone

pair electrons are stereochemically inactive in **1**-**5**; Bi-O distances and Bi-N distances are notably similar in each compound. The inactive lone pair may arise from the push-pull effect of the TTA ligand with an electron donating thiophene group and an electron withdrawing group of the CF_3 coupled with terpy binding that chelates the metal center.

For the homometallic bismuth phases the overall luminescence intensity followed the order **5** < **4** < **3**. This is consistent with prior observations that emission from bromobismuth species are often less intense than their chloride analogs.[35, 76] The emission peak attributed to TTA is much greater in intensity for **3 - 4** compared to **5**, which may be due to better efficiency of intraligand transitions. Analysis of the triplet state for TTA and terpy suggests that energy transfer from terpy to TTA is possible. Further, as the third emission band around 500-520 nm is not observed in **2**, it is likely this peak is related to influence of the halides present in the compounds as has been observed in bismuth-halide organic systems. Absent computational analysis, this emission band could result from a ligand-to-metal charge transfer (LMCT) between the Bi^{3+} and the halides[17, 44, 77], a ligand-to-ligand charge transfer (LLCT) between the halides and organic ligands[78], an intraligand (IL) phosphorescence induced by the heavy atom effect[35, 79, 80], or a metal-centered (MC) $s \rightarrow p$ transition[35, 81]. It would be expected that an IL phosphorescence or metal centered transition would also be observed in **2**, which is not the case. Bromo sp^2 metals have weaker reported luminescence than their chloride analogs due to increased sp/LMCT mixing, which could be an indication that LMCT is likely involved in the third emission band.[82] In **5**, this peak has a much greater intensity than for **3**-**4**, possibly owing to the presence of multiple halide ions rather than one that can be involved in charge transfer transitions.

The broad excitation window for the Eu-doped phases **2 – 5** compared to the slightly narrower excitation range for **6** likely results from incorporation into the bismuth host framework. Characteristic europium luminescence is observed upon excitation over a range of excitation wavelengths with no significant ligand contribution noted (Fig. S45). While β-diketonates can offer substantial sensitization for lanthanide-based systems,[47-49, 83] such enhanced photophysical properties are not achieved by doping lanthanide ions into the bismuth host compounds built from terpy and TTA that are reported here. In fact, all of the Eu doped phases exhibited low quantum efficiencies; the quantum yield of the nitrate containing compound was ~5% whereas the quantum yields of the halide containing compounds was less than 1%.

The absence of any ligand fluorescence in the emission spectra (contrasted to the strong ligand contribution observed in the bismuth-only compounds) suggests that the intramolecular energy transfer from the coordinated ligands to the Eu^{3+} metal ions is efficient for each doped phase except **$Bi_{0.999}Eu_{0.001}$-5**; however, **$Bi_{0.97}Eu_{0.03}$-2** has a notably lower quantum yield than **6**. If the observed decrease in luminescent efficiency between the Eu-doped phases and the Eu-only phase was exclusively due to poorly matched ligands, the φ_{tot} for **$Bi_{0.97}Eu_{0.03}$-2** and **6** should be comparable. However, the quantum yield of the Eu only phase (~15 %) is higher than that of the doped phases. This implies that the bismuth framework diminishes the overall quantum efficiency. This may arise from differences in the nonradiative decay pathways available in the Bi- and Eu-doped systems, and suggests that the effective sensitization routes for lanthanide-only compounds might be ineffective or ill-suited for lanthanide-doped bismuth-organic phases.

Attempts to synthesize the analogous lanthanide phases of **3** - **5** using identical synthetic methods proved unsuccessful, showing the varied differences between bismuth and lanthanide synthetic routes and highlighting the innate synthetic challenges of developing Ln-doped bismuth-organic materials. Further, while the Eu-only phase, **6**, displays the highest quantum yield in this paper, it is still low with respect to other europium- β-diketonates. Mazzanti et al. **$Bi_{0.97}Eu_{0.03}$-2** and **6** have reported a similar Eu(2,2′:6′,2″-terpyridine-6-carboxylate)$(TTA)_2$ species with a solid state quantum yield of 0.66(6).[49] Addition of the bound nitrate in **6** or absence of the carboxylate group on the terpy may be giving rise to the much lower solid state quantum yield reported here. Additionally, presence of the partially occupied methanol in the outer coordination sphere of **6** might act as a high energy oscillator, allowing for non-radiative deactivation processes.[84]

CONCLUSIONS

Five new monomeric bismuth and europium compounds built from terpyridine and 2-thenoyltrifluoroacetone and a bismuth dimer containing terpy and bridging methoxy groups were synthesized from methanol at room temperature. The stereochemically active $6s^2$ lone pair was not observed

in the crystal structures suggesting that judicious ligand selection may be an effective strategy towards controlling bismuth coordination chemistry and the manifestation of the lone pair electrons, in particular. Europium-doped phases of **2** – **5** were synthesized through careful addition of a europium salt aliquot to the reaction vial, ranging from 0.1 to 3% Eu^{3+} incorporation. Low doping percentages point to the inherent challenges of doping lanthanides into bismuth hosts. While the quantum efficiencies for all compounds, including the homometallic Eu phase were low, a relatively higher efficiency for the Eu-only (**6**) as compared to the Eu-doped Bi (**$Bi_{0.97}Eu_{0.03}$-2**) was observed. This may be attributed to the low percent Eu incorporated into the Bi host or may otherwise point to differences in the sensitization efficiencies, and nonradiative decay mechanisms in the homo- and heterometallic phases. The latter could have implications for the design of lanthanide sensitization in doped metal-organic compounds, particularly those based on ns^2 metal ions.

ASSOCIATED CONTENT

Supporting Information. Crystallographic refinement details, powder X-ray diffraction patterns, Raman spectra, TGA plots, and additional luminescence details are provided.

Notes

The manuscript was written through contributions of all authors. All authors have given their approval to the final version of the manuscript.

Conflicts of interest

There are no conflicts to declare.

Acknowledgments

The authors would like to gratefully acknowledge the Clare Booth Luce Foundation for their support. The authors would also like to thank the National Science Foundation for acquisition of the single crystal X-ray diffractometer (NSF CHE-1337975).

Corresponding Author

*E-mail: kek44@georgetown.edu (KEK)

ORCID

Alyssa K. Adcock: 0000-0001-9977-3756

Jeffery A. Bertke: 0000-0002-3419-5163

Karah E. Knope: 0000-0002-5690-715X

REFERENCES

1. Zhang, Y.; Yuan, S.; Day, G.; Wang, X.; Yang, X.; Zhou, H.-C., Luminescent sensors based on metal-organic frameworks. *Coordination Chemistry Reviews* **2018,** *354*, 28-45.
2. Bai, G.; Tsang, M.-K.; Hao, J., Luminescent Ions in Advanced Composite Materials for Multifunctional Applications. *Advanced Functional Materials* **2016,** *26* (35), 6330-6350.
3. Feldmann, C.; Jüstel, T.; Ronda, C. R.; Schmidt, P. J., Inorganic Luminescent Materials: 100 Years of Research and Application. *Advanced Functional Materials* **2003,** *13* (7), 511-516.
4. Mukherjee, S.; Thilagar, P., Recent advances in purely organic phosphorescent materials. *Chemical Communications* **2015,** *51* (55), 10988-11003.
5. Binnemans, K., Lanthanide-Based Luminescent Hybrid Materials. *Chemical Reviews* **2009,** *109* (9), 4283-4374.
6. Lustig, W. P.; Li, J., Luminescent metal–organic frameworks and coordination polymers as alternative phosphors for energy efficient lighting devices. *Coordination Chemistry Reviews* **2018,** *373*, 116-147.

7. Maurer, L. A.; Pearce, O. M.; Maharaj, F. D. R.; Brown, N. L.; Amador, C. K.; Damrauer, N. H.; Marshak, M. P., Open for Bismuth: Main Group Metal-to-Ligand Charge Transfer. *Inorganic Chemistry* **2021,** *60* (14), 10137-10146.
8. Parke, S. M.; Narreto, M. A. B.; Hupf, E.; McDonald, R.; Ferguson, M. J.; Hegmann, F. A.; Rivard, E., Understanding the Origin of Phosphorescence in Bismoles: A Synthetic and Computational Study. *Inorganic Chemistry* **2018,** *57* (13), 7536-7549.
9. Batrice, R. J.; Ayscue III, R. L.; Adcock, A. K.; Sullivan, B. R.; Han, S. Y.; Piccoli, P. M.; Bertke, J. A.; Knope, K. E., Photoluminescence of Visible and NIR-Emitting Lanthanide-Doped Bismuth-Organic Materials. *Chemistry – A European Journal* **2018,** *24* (21), 5630-5636.
10. Sorg, J. R.; Schneider, T.; Wohlfarth, L.; Schäfer, T. C.; Sedykh, A.; Müller-Buschbaum, K., Sb- and Bi-based coordination polymers with N-donor ligands with and without lone-pair effects and their photoluminescence properties. *Dalton Transactions* **2020,** *49* (15), 4904-4913.
11. Ayscue, R. L.; Vallet, V.; Bertke, J. A.; Réal, F.; Knope, K. E., Structure–Property Relationships in Photoluminescent Bismuth Halide Organic Hybrid Materials. *Inorganic Chemistry* **2021,** *60* (13), 9727-9744.
12. Briand, G. G.; Burford, N., Bismuth Compounds and Preparations with Biological or Medicinal Relevance. *Chemical Reviews* **1999,** *99* (9), 2601-2658.
13. Keogan, D.; Griffith, D., Current and Potential Applications of Bismuth-Based Drugs. *Molecules* **2014,** *19* (9), 15258.
14. Yang, N.; Sun, H., Biocoordination chemistry of bismuth: Recent advances. *Coordination Chemistry Reviews* **2007,** *251* (17–20), 2354-2366.
15. Leonard, N. M.; Wieland, L. C.; Mohan, R. S., Applications of bismuth(III) compounds in organic synthesis. *Tetrahedron* **2002,** *58* (42), 8373-8397.
16. Folkerts, H. F.; Zuidema, J.; Blasse, G., Different types of s_2 ion luminescence in compounds with eulytite structure. *Chemical Physics Letters* **1996,** *249* (1), 59-63.
17. Srivastava, A. M.; Beers, W. W., On the impurity trapped exciton luminescence in $La_2Zr_2O_7:Bi^{3+}$. *Journal of Luminescence* **1999,** *81* (4), 293-300.
18. Ollevier, T., New trends in bismuth-catalyzed synthetic transformations. *Organic & Biomolecular Chemistry* **2013,** *11* (17), 2740-2755.
19. Wang, Q.-X.; Li, G., Bi(III) MOFs: syntheses, structures and applications. *Inorganic Chemistry Frontiers* **2021,** *8* (3), 572-589.
20. Xu, L.-J.; Lin, X.; He, Q.; Worku, M.; Ma, B., Highly efficient eco-friendly X-ray scintillators based on an organic manganese halide. *Nature Communications* **2020,** *11* (1), 4329.
21. Groom, C. R.; Bruno, I. J.; Lightfoot, M. P.; Ward, S. C., The Cambridge Structural Database. *Acta Crystallographica Section B* **2016,** *72* (2), 171-179.
22. Wibowo, A. C.; Smith, M. D.; zur Loye, H.-C., New 3D bismuth-oxo coordination polymers containing terephthalate-based ligands: observation of Bi2O2-layer and Bi4O3-chain motifs. *CrystEngComm* **2011,** *13* (2), 426-429.
23. Adcock, A. K.; Gibbons, B.; Einkauf, J. D.; Bertke, J. A.; Rubinson, J. F.; de Lill, D. T.; Knope, K. E., Bismuth(III)-thiophenedicarboxylates as host frameworks for lanthanide ions: synthesis, structural characterization, and photoluminescent behavior. *Dalton Transactions* **2018,** *47* (38), 13419-13433.
24. Wibowo, A. C.; Vaughn, S. A.; Smith, M. D.; zur Loye, H.-C., Novel Bismuth and Lead Coordination Polymers Synthesized with Pyridine-2,5-Dicarboxylates: Two Single Component "White" Light Emitting Phosphors. *Inorganic Chemistry* **2010,** *49* (23), 11001-11008.
25. Wibowo, A. C.; Smith, M. D.; zur Loye, H.-C., Structural Diversity of Metal–Organic Materials Containing Bismuth(III) and Pyridine-2,5-Dicarboxylate. *Crystal Growth & Design* **2011,** *11* (10), 4449-4457.

26. Jolas, J. L.; Hoppe, S.; Whitmire, K. H., Oligomerization and Oxide Formation in Bismuth Aryloxides: Synthesis, Characterization, and Structures of $[NaBi(OC_6F_5)_4(THF)]_\infty$ and $Na_4Bi_2(\mu_6\text{-}O)(OC_6F_5)_8(THF)_4$. *Inorganic Chemistry* **1997,** *36* (15), 3335-3340.
27. Sushrutha, S. R.; Natarajan, S., Bismuth Carboxylates with Brucite- and Fluorite-Related Structures: Synthesis Structure and Properties. *Crystal Growth & Design* **2013,** *13* (4), 1743-1751.
28. Mohan, R., Green bismuth. *Nature Chemistry* **2010,** *2* (4), 336-336.
29. Wibowo, A. C.; Smith, M. D.; zur Loye, H.-C., A new Kagomé lattice coordination polymer based on bismuth and pyridine-2,5-dicarboxylate: structure and photoluminescent properties. *Chemical Communications* **2011,** *47* (26), 7371-7373.
30. Heine, J.; Wehner, T.; Bertermann, R.; Steffen, A.; Müller-Buschbaum, K., $^2{}_\infty[Bi_2Cl_6(pyz)_4]$: A 2D-Pyrazine Coordination Polymer As Soft Host Lattice for the Luminescence of the Lanthanide Ions Sm^{3+}, Eu^{3+}, Tb^{3+}, and Dy^{3+}. *Inorganic Chemistry* **2014,** *53* (14), 7197-7203.
31. Zhang, X.-P.; Tian, H.-R.; Yan, G.-F.; Su, Y.; Feng, Y.-L.; Cheng, J.-W., Incorporating different secondary building units of {Bi2}, {Bi8} and {Bi10} to construct diversity of luminescent bismuth-organic frameworks. *Dalton Transactions* **2013,** *42* (4), 1088-1093.
32. Thirumurugan, A.; Cheetham, A. K., Anionic Metal–Organic Frameworks of Bismuth Benzenedicarboxylates: Synthesis, Structure and Ligand-Sensitized Photoluminescence. *European Journal of Inorganic Chemistry* **2010,** *2010* (24), 3823-3828.
33. Feyand, M.; Köppen, M.; Friedrichs, G.; Stock, N., Bismuth Tri- and Tetraarylcarboxylates: Crystal Structures, In Situ X-ray Diffraction, Intermediates and Luminescence. *Chemistry – A European Journal* **2013,** *19* (37), 12537-12546.
34. Shen, N.; Li, J.; Wu, Z.; Hu, B.; Cheng, C.; Wang, Z.; Gong, L.; Huang, X., α- and β-[Bmim][$BiCl_4$(2,2′-bpy)]: Two Polymorphic Bismuth-Containing Ionic Liquids with Crystallization-Induced Phosphorescence. *Chemistry – A European Journal* **2017,** *23* (62), 15795-15804.
35. Toma, O.; Mercier, N.; Botta, C., N-Methyl-4,4′-bipyridinium and N-Methyl-N′-oxide-4,4′-bipyridinium Bismuth Complexes – Photochromism and Photoluminescence in the Solid State. *European Journal of Inorganic Chemistry* **2013,** *2013* (7), 1113-1117.
36. Thirumurugan, A.; Li, W.; Cheetham, A. K., Bismuth 2,6-pyridinedicarboxylates: Assembly of molecular units into coordination polymers, CO_2 sorption and photoluminescence. *Dalton Transactions* **2012,** *41* (14), 4126-4134.
37. Yu, X.; Zhang, H.; Cao, Y.; Hu, Z.; Chen, Y.; Wang, Z., Two novel 3-D bismuth oxalates with organic amines protruding in channels. *Journal of Solid State Chemistry* **2006,** *179* (10), 3095-3100.
38. Kan, L.; Li, J.; Luo, X.; Li, G.; Liu, Y., Three novel bismuth-based coordination polymers: Synthesis, structure and luminescent properties. *Inorganic Chemistry Communications* **2017,** *85*, 70-73.
39. Al-Nubi, M. A. A.; Hamisu, A. M.; Ariffin, A.; Zhang, J.; Shimizu, G. K. H.; Jo, H.; Ok, K. M.; Wibowo, A. C., A new bismuth coordination polymer with proton conductivity and orange-red photoluminescence. *Journal of Coordination Chemistry* **2021,** *74* (11), 1810-1822.
40. Jin, J.-C.; Lin, Y.-P.; Wu, Y.-H.; Gong, L.-K.; Shen, N.-N.; Song, Y.; Ma, W.; Zhang, Z.-Z.; Du, K.-Z.; Huang, X.-Y., Long lifetime phosphorescence and X-ray scintillation of chlorobismuthate hybrids incorporating ionic liquid cations. *Journal of Materials Chemistry C* **2021,** *9* (5), 1814-1821.
41. Zhang, X.-P.; Wang, D.-G.; Su, Y.; Tian, H.-R.; Lin, J.-J.; Feng, Y.-L.; Cheng, J.-W., Luminescent 2D bismuth–cadmium–organic frameworks with tunable and white light emission by doping different lanthanide ions. *Dalton Transactions* **2013,** *42* (29), 10384-10387.

42. Xu, L.; Xu, Y.; Li, X.; Wang, Z.; Sun, T.; Zhang, X., Eu^{3+}/Tb^{3+} functionalized Bi-based metal–organic frameworks toward tunable white-light emission and fluorescence sensing applications. *Dalton Transactions* **2018,** *47* (46), 16696-16703.
43. Cunha, C. S.; Köppen, M.; Terraschke, H.; Friedrichs, G.; Malta, O. L.; Stock, N.; Brito, H. F., Luminescence tuning and single-phase white light emitters based on rare earth ions doped into a bismuth coordination network. *Journal of Materials Chemistry C* **2018,** *6* (46), 12668-12678.
44. Sorg, J. R.; Wehner, T.; Matthes, P. R.; Sure, R.; Grimme, S.; Heine, J.; Müller-Buschbaum, K., Bismuth as a versatile cation for luminescence in coordination polymers from BiX_3/4,4′-bipy: understanding of photophysics by quantum chemical calculations and structural parallels to lanthanides. *Dalton Transactions* **2018,** *47* (23), 7669-7681.
45. Batrice, R. J.; Ridenour, J. A.; Ayscue Iii, R. L.; Bertke, J. A.; Knope, K. E., Synthesis, structure, and photoluminescent behaviour of molecular lanthanide–2-thiophenecarboxylate–2,2′:6′,2′′-terpyridine materials. *CrystEngComm* **2017,** *19* (35), 5300-5312.
46. de Bettencourt-Dias, A.; Barber, P. S.; Viswanathan, S., Aromatic N-donor ligands as chelators and sensitizers of lanthanide ion emission. *Coordination Chemistry Reviews* **2014,** *273-274*, 165-200.
47. Binnemans, K., Rare-earth beta-diketonates. In *Handbook on the Physics and Chemistry of Rare Earths*, Gschneidner, K. A. J., Bünzli, J.-C.G.; Pecharsky, V.K., Ed. Elsevier B.V: 2005; Vol. 35, pp 107-272.
48. Freund, C.; Porzio, W.; Giovanella, U.; Vignali, F.; Pasini, M.; Destri, S.; Mech, A.; Di Pietro, S.; Di Bari, L.; Mineo, P., Thiophene Based Europium β-Diketonate Complexes: Effect of the Ligand Structure on the Emission Quantum Yield. *Inorganic Chemistry* **2011,** *50* (12), 5417-5429.
49. Andreiadis, E. S.; Gauthier, N.; Imbert, D.; Demadrille, R.; Pécaut, J.; Mazzanti, M., Lanthanide Complexes Based on β-Diketonates and a Tetradentate Chromophore Highly Luminescent as Powders and in Polymers. *Inorganic Chemistry* **2013,** *52* (24), 14382-14390.
50. *SAINT*, Bruker AXS Inc.: Madison, WI, USA, 2007.
51. *APEX2*, Bruker AXS Inc.: Madison, WI, USA, 2008.
52. Wang, J.-G.; Huang, C.-C.; Huang, X.-H.; Liu, D.-S., Three-Dimensional Lanthanide Thiophenedicarboxylate Framework with an Unprecedented (4,5)-Connected Topology. *Crystal Growth & Design* **2008,** *8* (3), 795-798.
53. Sheldrick, G., A short history of SHELX. *Acta Crystallographica Section A* **2008,** *64* (1), 112-122.
54. Hubschle, C. B.; Sheldrick, G. M.; Dittrich, B., ShelXle: a Qt graphical user interface for SHELXL. *Journal of Applied Crystallography* **2011,** *44* (6), 1281-1284.
55. *CRC Handbook of Chemistry and Physics*. 91st ed.; CRC Press: Boca Raton, FL, 2010.
56. Yin, S.-F.; Shimada, S., Synthesis and structure of bismuth compounds bearing a sulfur-bridged bis(phenolato) ligand and their catalytic application to the solvent-free synthesis of propylene carbonate from CO_2 and propylene oxide. *Chemical Communications* **2009,** (9), 1136-1138.
57. Sadeghi Roodsari, M.; Shaabani, B.; Mirtamizdoust, B.; Dusek, M.; Fejfarova, K., Sonochemical Synthesis of Bismuth(III) Nano Coordination Compound and Direct Synthesis of Bi_2O_3 Nanoparticles from a Bismuth(III) Nano Coordination Compound Precursor. *Journal of Inorganic and Organometallic Polymers and Materials* **2015,** *25* (5), 1226-1232.
58. Spek, A., Structure validation in chemical crystallography. *Acta Crystallographica Section D* **2009,** *65* (2), 148-155.
59. Steiner, T., Unrolling the hydrogen bond properties of C–H···O interactions. *Chemical Communications* **1997,** (8), 727-734.
60. Steiner, T., The Hydrogen Bond in the Solid State. *Angewandte Chemie International Edition* **2002,** *41* (1), 48-76.

61. Metrangolo, P.; Resnati, G., Halogen Bonding: A Paradigm in Supramolecular Chemistry. *Chemistry – A European Journal* **2001,** *7* (12), 2511-2519.
62. Swierczynski, D.; Luboradzki, R.; Dolgonos, G.; Lipkowski, J.; Schneider, H.-J., Non-Covalent Interactions of Organic Halogen Compounds with Aromatic Systems – Analyses of Crystal Structure Data. *European Journal of Organic Chemistry* **2005,** *2005* (6), 1172-1177.
63. A. Bowmaker, G.; M. M. Hannaway, F.; C. Junk, P.; Lee, A.; W. Skelton, B.; H. White, A., Synthetic, Structural and Vibrational Spectroscopic Studies in Bismuth(III) Halide/N,N'-Aromatic Bidentate Base Systems. V Bismuth(III) Halide/N,N'-Bidentate Ligand (1 : 2) Systems. *Australian Journal of Chemistry* **1998,** *51*.
64. Adonin, S. A.; Rakhmanova, M. I.; Samsonenko, D. G.; Sokolov, M. N.; Fedin, V. P., Hybrid salts of binuclear Bi(III) halide complexes with 1,2-bis(pyridinium)ethane cation: Synthesis, structure and luminescent behavior. *Inorganica Chimica Acta* **2016,** *450*, 232-235.
65. Nekoei, A.-R.; Tayyari, S. F.; Vakili, M.; Holakoei, S.; Hamidian, A. H.; Sammelson, R. E., Conformation and vibrational spectra and assignment of 2-thenoyltrifluoroacetone. *Journal of Molecular Structure* **2009,** *932* (1), 112-122.
66. A. Harwig, H., *On the Structure of Bismuthsesquioxide: The α, β, γ, and δ-phase*. 1978; Vol. 444, p 151-166.
67. Eggenweiler, U.; Keller, E.; Kramer, V., Redetermination of the crystal structures of the `Arppe compound' $Bi_{24}O_{31}Cl_{10}$ and the isomorphous $Bi_{24}O_{31}Br_{10}$. *Acta Crystallographica Section B* **2000,** *56* (3), 431-437.
68. Yang, S.; Sheng, G.; Montavon, G.; Guo, Z.; Tan, X.; Grambow, B.; Wang, X., Investigation of Eu(III) immobilization on γ-Al2O3 surfaces by combining batch technique and EXAFS analyses: Role of contact time and humic acid. *Geochimica et Cosmochimica Acta* **2013,** *121*, 84-104.
69. Marcantonatos, M. D.; Deschaux, M.; Vuilleumier, J.-J., Interactions of aqueous 7F and 5D1 europium(III) ions with bromide and inner-sphere coordination exciplex formation. *Journal of the Chemical Society, Faraday Transactions 2: Molecular and Chemical Physics* **1984,** *80* (12), 1569-1598.
70. Mürner, H.-R.; Chassat, E.; Thummel, R. P.; Bünzli, J.-C. G., Strong enhancement of the lanthanide-centred luminescence in complexes with 4-alkylated 2,2';6',2''-terpyridines. *Journal of the Chemical Society, Dalton Transactions* **2000,** (16), 2809-2816.
71. Junk, P. C.; Louis, L. M., Dimeric Structure of $[(\eta_2\text{-}NO_3)_2(tpy)Bi(\mu\text{-}OH)_2Bi(tpy)(\eta_2\text{-}NO_3)_2]$. *Zeitschrift für anorganische und allgemeine Chemie* **2000,** *626* (2), 556-559.
72. Tershansy, M. A.; Goforth, A. M.; Smith, M. D.; zur Loye, H.-C., The Synthesis and Crystal Structure of $[BiI_2(tpy)_2][Bi_2I_7(tpy)]$: A New Metal Halide Material. *Journal of Chemical Crystallography* **2008,** *38* (6), 453-459.
73. Raston, C. L.; Rowbottom, G. L.; White, A. H., Structural studies of Group 5B–halide–dithio-ligand complexes. Part 7. Crystal structures of the 1 : 1 adducts of (NN-diethyldithiocarbamato)-di-iodobismuth(III) with 2,2'-bipyridyl and 2,2':6',2''-terpyridyl. *Journal of the Chemical Society, Dalton Transactions* **1981,** (6), 1383-1388.
74. Lewis, K. M.; Kelley, J.; Peterson, L.; Smith, M. D.; Severance, R. C.; Vaughn, S. A.; Loye, H.-C. z., Synthesis and Crystal Structure of an Iodobismuthate Incorporating Both a Cationic and Anionic Bi (III) Complex Ion. *Journal of Chemical Crystallography* **2010,** *40* (10), 867-871.
75. Adcock, A. K.; Batrice, R. J.; Bertke, J. A.; Knope, K. E., Structural Diversity of Bismuth(III) Thiophenemonocarboxylates Isolated from Aqueous Solutions. *European Journal of Inorganic Chemistry* **2017,** *2017* (11), 1435-1445.
76. Adonin, S. A.; Sokolov, M. N.; Fedin, V. P., Polynuclear halide complexes of Bi(III): From structural diversity to the new properties. *Coordination Chemistry Reviews* **2016,** *312*, 1-21.

77. Wolfert, A.; Blasse, G., Luminescence of Bi3+-doped crystals of Cs2NaYBr6 and Cs2NaLaCl6. *Journal of Solid State Chemistry* **1985,** *59* (2), 133-142.
78. Chen, W.-T.; Huang, J.-G.; Yi, X.-G., In Situ Preparation, Structure, Photoluminescence and Theoretical Study of an Unusual Bismuth Complex. *2016* **2016,** *63* (4), 6.
79. Strasser, A.; Vogler, A., Optical properties of thallium(I), lead(II) and bismuth(III) hexafluoroacetylacetonates. Intraligand phosphorescence under ambient conditions. *Inorganic Chemistry Communications* **2004,** *7* (4), 528-530.
80. Strasser, A.; Vogler, A., Intraligand phosphorescence of lead(II) β-diketonates under ambient conditions. *Journal of Photochemistry and Photobiology A: Chemistry* **2004,** *165* (1), 115-118.
81. Zhu, X.; Li, X.; Liu, Q.; Lü, J.; Guo, Z.; He, J.; Li, Y.; Cao, R., Two luminescent frameworks constructed from lead(II) salts with carboxylate ligands containing dinuclear lead(II) units. *Journal of Solid State Chemistry* **2007,** *180* (8), 2386-2392.
82. Oldenburg, K.; Vogler, A., Electronic Spectra and Photochemistry of Tin(II), Lead(II), Antimony(III), and Bismuth(III) Bromide Complexes in Solution. In *Zeitschrift für Naturforschung B*, 1993; Vol. 48, p 1519.
83. Lima, N. B. D.; Gonçalves, S. M. C.; Júnior, S. A.; Simas, A. M., A Comprehensive Strategy to Boost the Quantum Yield of Luminescence of Europium Complexes. *Scientific Reports* **2013,** *3*, 2395.
84. Stein, G.; Würzberg, E., Energy gap law in the solvent isotope effect on radiationless transitions of rare earth ions. *The Journal of Chemical Physics* **1975,** *62* (1), 208-213.